

PACS numbers: 42.55.Lt; 42.55.Rz; 42.60.By; 42.65.Jx; 42.65.Ky; 52.50.Jm
DOI: 10.1070/QE2013v043n04ABEH013559

Production of extended plasma channels in atmospheric air by amplitude-modulated UV radiation of GARPUN-MTW Ti:sapphire–KrF laser. Part 2. Accumulation of plasma electrons and electric discharge control

V.D. Zvorykin, A.A. Ionin, A.O. Levchenko, G.A. Mesyats, L.V. Seleznev, D.V. Sinitsyn, I.V. Smetanin, E.A. Sunchugasheva, N.N. Ustinovskii, A.V. Shutov

Abstract. **The problem of the production of extended (~1 m) plasma channels is studied in atmospheric air by amplitude-modulated laser pulses of UV radiation, which are a superposition of a subpicosecond USP train amplified in a regenerative KrF amplifier with an unstable confocal resonator and a quasi-stationary lasing pulse. The USPs possess a high (0.2–0.3 TW) peak power and efficiently ionise oxygen molecules due to multiphoton ionisation, and the quasi-stationary lasing pulse, which has a relatively long duration (~100 ns), maintains the electron density at a level $n_e = (3–5) \times 10^{14}$ cm^{-3} by suppressing electron attachment to oxygen. Experiments in laser triggering of high-voltage electric discharges suggest that the use of combined pulses results in a significant lowering of the breakdown threshold and enables controlling the discharge trajectory with a higher efficiency in comparison with smooth pulses. It was shown that controlled breakdowns may develop with a delay of tens of microseconds relative to the laser pulse, which is many orders of magnitude greater than the lifetime of free electrons in the laser-induced plasma. We propose a mechanism for this breakdown, which involves speeding-up of the avalanche ionisation of the air by negative molecular oxygen ions with a low electron binding energy (~0.5 eV) and a long lifetime (~1 ms), which are produced upon cessation of the laser pulse.**

Keywords: *high-voltage discharge, discharge guiding, laser discharge triggering, plasma channels in the atmosphere, air ionisation by laser radiation.*

1. Extended plasma channels in atmospheric air produced by laser radiation for electric discharge control

There are two radically different approaches to the control over long-range high-voltage electric discharges in the atmosphere by producing conductive plasma channel with lasers. The first approach consists in producing the so-called laser spark inside a discharge gap – a dense plasma with a high ion temperature. For instance, for long-wavelength CO_2 laser radiation (λ = 10.6 μm) the threshold for the optical air breakdown (not higher than 10^9 W cm^{-2}) is lower than for UV radiation, and in the course of avalanche ionisation it produces a relatively long-living dense plasma with an electron density $n_e \approx 10^{19}$ cm^{-3}, which is close to the thermodynamic equilibrium state with the electron temperature approximately equal to the ion temperature ($T_e \approx T_i \approx 1$ eV) [1]. The stochasticity of the optical breakdown, which is caused by aerosol particles, random fluctuations in intensity distribution, and plasma-induced reflectin of radiation, gives rise to the structural discreteness of a long laser spark obtained when the radiation is focused with long-focus optics. This does not permit using in full measure the high electrical conduction of this plasma for discharge triggering [2]. Continuous plasma channels may be obtained in the focusing of pulsed laser radiation with conical optics [3] or, in the case of a pulse-periodic laser, in the translation of the optical system's focus due to the motion of one of the mirrors of a ground-based telescope [4], or in the spatial motion of the focusing system itself due to the jet thrust produced under laser irradiation of support platform [5]. In the presence of dense equilibrium plasma the electrical breakdown voltage of long gaps is tens of times lower, although the energy expenses for its production are known to be high: apart from the energy $\sim n_e I_i$ (where I_i is the ionisation potential) that goes to ionise the gas, they include the energy spent to heat ions and electrons to the equilibrium temperature. The experimentally measured energy expenses amount to ~200 J per one metre of plasma channel length [3]. A ~20-m long channel, which is capable of initiating a lightning discharge according to the estimates of Ref. [6], requires a pulsed CO_2 laser with an energy of ~5 kJ [3, 5].

The other approach to the problem involves the use of femto- or picosecond-long USPs of multiterawatt peak power generated by a titanium-sapphire laser in the near-IR wavelength range (with the band centre at λ = 790 nm) [7, 8] or a hybrid Ti:sapphire–KrF laser system in the UV range (λ = 248 nm) [9–11]. During the propagation through the air, the USP laser beam disintegrates, owing to the Kerr nonlinearity, into many separate filamentary channels with a characteristic diameter of ~100 μm and a local electron density $n_e = 10^{16}–10^{17}$ cm^{-3}. The filaments in which the Kerr focusing is compensated by radiation defocusing on the radial electron density profile and partly by radiation diffraction transmit an intensity of $10^{13}–10^{14}$ W cm^{-2} in a self-consistent regime (see, for instance, Refs [12–14]). In case of a titanium-sapphire

V.D. Zvorykin, A.A. Ionin, A.O. Levchenko, G.A. Mesyats, L.V. Seleznev, D.V. Sinitsyn, I.V. Smetanin, E.A. Sunchugasheva, N.N. Ustinovskii, A.V. Shutov P.N. Lebedev Physics Institute, Russian Academy of Sciences, Leninsky prosp. 53, 119991 Moscow, Russia; e-mail: zvorykin@sci.lebedev.ru

Received 30 January 2013; revision received 12 February 2013
Kvantovaya Elektronika **43** (4) 339–346 (2013)
Translated by E.N. Ragozin

laser with laser pulses at an energy of several hundred millijoules and a peak power of several terawatts, the length of such plasma filaments may range up to hundreds of metres, although their conductivity is many orders of magnitude lower than the conductivity of optical air breakdown plasma. In the high-intensity laser field, in the filaments there occurs multiphoton ionisation of the gas (primarily of O_2 molecules, which possess the lowest (I_i = 12.06 eV) ionisation potential among the air components). The detached photoelectrons acquire an energy of the order of an electronvolt; in this case, the electron and ion temperatures do not manage to change significantly during the short ionisation time, i.e. $T_e \gg T_i$, and a rapid relaxation of this nonequilibrium plasma proceeds upon cessation of the laser pulse. For a high electron density in the filaments ($n_e \geqslant n_e^* = 10^{14} \times 10^{15}$ cm^{-3}), there dominates an electron-ion dissociative recombination, which limits the electron lifetime τ_e to several nanoseconds [12–14]. Under these conditions, the USP-induced electron conduction persists in a relatively short filament length ($l_e = c\tau_e \approx 1$ m), this domain travelling with the velocity of light c after the laser pulse. As a consequence, in numerous experiments with femtosecond pulses [15–28] the longest controlled discharge length did not exceed 4 m even for a megavolt voltage [20], which is much shorter than the filament length.

To lengthen the controlled discharge requires increasing the ionisation time, for instance, with the use of a train of USPs, each of which produces a new portion of photoelectrons [29, 30]; in this case, the pulse separation in the train must be of the order of the free-electron lifetime. Another possibility for maintaining the conductivity in the photoionisation plasma emerges at a later relaxation stage, when the electron attachment to oxygen molecules with the formation of negative O_2^- ions begins to dominate owing to a lowering of the electron density, so that $n_e \leqslant n_e^*$. The characteristic electron lifetime in this case increases to several tens of nanoseconds, depending on the electron temperature and the applied electric field [6, 30]. Since the electron binding energy ε in O_2^-, which is equal to ~0.5 eV, is considerably lower than the ionisation potential I_i of oxygen molecules, the weakly bound electrons may be released with small energy expenses in the course of photodetachment by visible or UV radiation, this being possible for considerably lower radiation intensities attainable in longer pulses. This requires a combination of USPs, which efficiently produce primary photoelectrons, and a long pulse, which compensates for attachment and maintains the free-electron density in the plasma at a level $n_e \approx n_e^*$ [9, 31, 32]. For high intensities, the second longer and higher-energy pulse may multiply electrons in an avalanche manner up to the optical air breakdown ($n_e \approx 10^{19}$ cm^{-3}) due to inverse bremsstrahlung of laser radiation in the less dense plasma produced by the USPs [33–36].

KrF lasers offer several potential advantages in the implementation of the approaches discussed above.

1. As shown in the first part of our present work [37], their active medium recovers rapidly ($\tau_c \approx 2$ ns) after the passage of a USP. This makes it possible to efficiently amplify USP trains with a pulse separation $\Delta t \approx \tau_c$ comparable to the short time of electron density relaxation in the photoionisation plasma. Generated in the regenerative amplification scheme simultaneously with USPs is a high-energy pulse, whose duration τ_{long} is determined by the duration of the laser pump pulse ($\tau_{long} \approx \tau_p$). Therefore, obtaining combined pulses does not require an additional laser, and bringing the USPs and long pulses into temporal and spatial coincidence is made considerably simpler.

2. Since the peak power of amplitude-modulated UV radiation pulses (0.2–0.3 TW) is several orders of magnitude higher than the critical power for filamentation $P_{cr} \approx 0.1$ GW (λ = 248 nm), the laser beam undergoes multiple small-scale filamentation even at the laser output. However, in this case it does not produce a long self-maintaining channel caused by nonlinear focusing, which is typical for IR radiation filamentation. Therefore, USPs and long pulses automatically terminate along the propagation path [38]. To spatially overlap the extended domain of nonlinear USP focusing and the pulses of an auxiliary laser in the case of a titanium-sapphire laser, use should be made of an axicon, which focusing the radiation onto a segment [33–36].

3. The effective cross section for the multiphoton ionisation of oxygen molecules by UV KrF laser radiation is far greater than the similar cross section for the ionisation by IR radiation [39]. The cross section for the photodetachment of electrons from O_2^- ions with a resonance peak $\sigma_{ph} \approx 10^{-17}$ cm^2 at λ = 248 nm is also much greater than in the case of IR radiation [40, 41].

In continuation of Ref. [42], the present work is an investigation of air ionisation by combined (amplitude-modulated) 100-ns long UV radiation pulses generated by the GARPUN-MTW hybrid Ti:sapphire–KrF laser system. We demonstrated efficient control over extended high-voltage electric discharges with the help of plasma channels produced in the atmosphere.

2. Air ionisation by amplitude-modulated laser pulses

To determine the electron density in the photoionisation plasma produced by UV laser radiation in the atmospheric air, advantage was taken, like in earlier experiments [32, 42, 43], of a photoelectric technique which relies on measurements of the electric current between two annular electrodes (Fig. 1). The amplitude-modulated radiation pulses were generated by the GARPUN-MTW hybrid Ti:sapphire–KrF laser system. The system was operated in the regime of regenerative amplification of single USPs or USP trains injected into the unstable telescopic resonator of a wide-aperture KrF amplifier with electric-beam pumping [37]. To obtain a slightly converging laser beam (to reduce the beam aperture and the size of optics in use) at the amplifier output, the resonator was

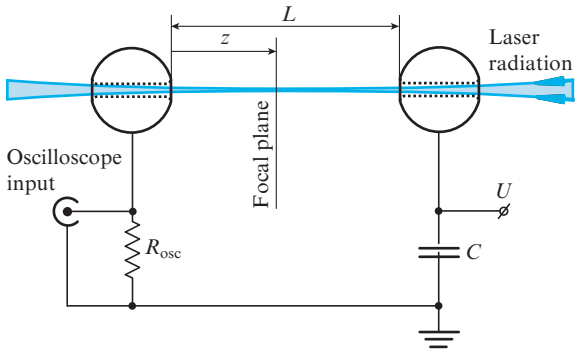

Figure 1. Schematic representation of photoelectric measurements of the electron plasma density.

somewhat lengthened relative to the nominal value. In the subsequent beam focusing with a spherical mirror with a focal length $F = 8$ m, the focal beam waist was located at a distance of 6.75 m from the mirror. The position of the geometrical focus of the resonator–spherical mirror optical system was determined in the alignment of the entire optical path of the facility using the USPs of UV radiation generated by the titanium-sapphire starting complex, but without pumping the KrF amplifiers. Two spherical electrodes 5 cm in diameter spaced at a distance $L = 20$ cm were located in line with the laser beam. To eliminate the photoeffect on the electrodes, they had opening 1 cm in diameter, through which the laser radiation was transmitted. A constant voltage $U = 5–22$ kV was applied to one of the electrodes, the other was loaded onto the 50-Ω input of a Tektronix TDS-3054 four channel digital oscilloscope with a sampling frequency of 5 GHz. Applied to the adjacent oscilloscope input was the signal from a Thorlabs DET 210 photodiode, which recorded the laser radiation pulse with a resolution of ~1 ns. As suggested by preliminary experiments, for the same laser pulses the photocurrent signals were proportional to the applied voltage U and inversely proportional to the gap length L, i.e. Ohm's law was fulfilled. This provided the possibility to determine the conductivity of the plasma channel proceeding from photocurrent measurements. The temporal resolution of the measurement setup was estimated at ~1 ns.

Figure 2 shows typical waveforms of the photocurrent in the plasma channel obtained for a voltage $U = 15$ kV across the interelectrode gap when the geometrical beam focus was located near the distant (relative to the direction of radiation propagation) grounded electrode (see Fig. 1). Also shown in Fig. 2 are the waveforms of laser pulses for different operating regimes of the regenerative amplifier. In the absence of USP injection into the unstable resonator, the laser generated a smooth ~100-ns long radiation pulse with an energy of ~15 J. In this case, the amplitude of photocurrent signal did not exceed 0.3 V (Fig. 2a). When a single USP was injected into the resonator, the output radiation pulse had the same energy and duration, but was modulated by the USP executing successive passages through the resonator with an interval of 17 ns. The USPs, which had a duration of ~1 ps [10, 11], were integrated by the photodiode in the waveforms, with the result that their peak power in the waveforms was 1000 times lower than the true one, which exceeded the power of quasi-stationary lasing by about the same factor [37]. In this case, the photocurrent signal was a sequence of several peaks with amplitudes of up to 20 V synchronised to the USPs (Fig. 2b). The FWHM duration of the photocurrent peaks was equal to ~2 ns, which corresponds to the characteristic electron–ion recombination time in our nonequilibrium plasma (see Section 1). When a train of USPs spaced at intervals of 5.3 ns, which was comparable to the population inversion recovery

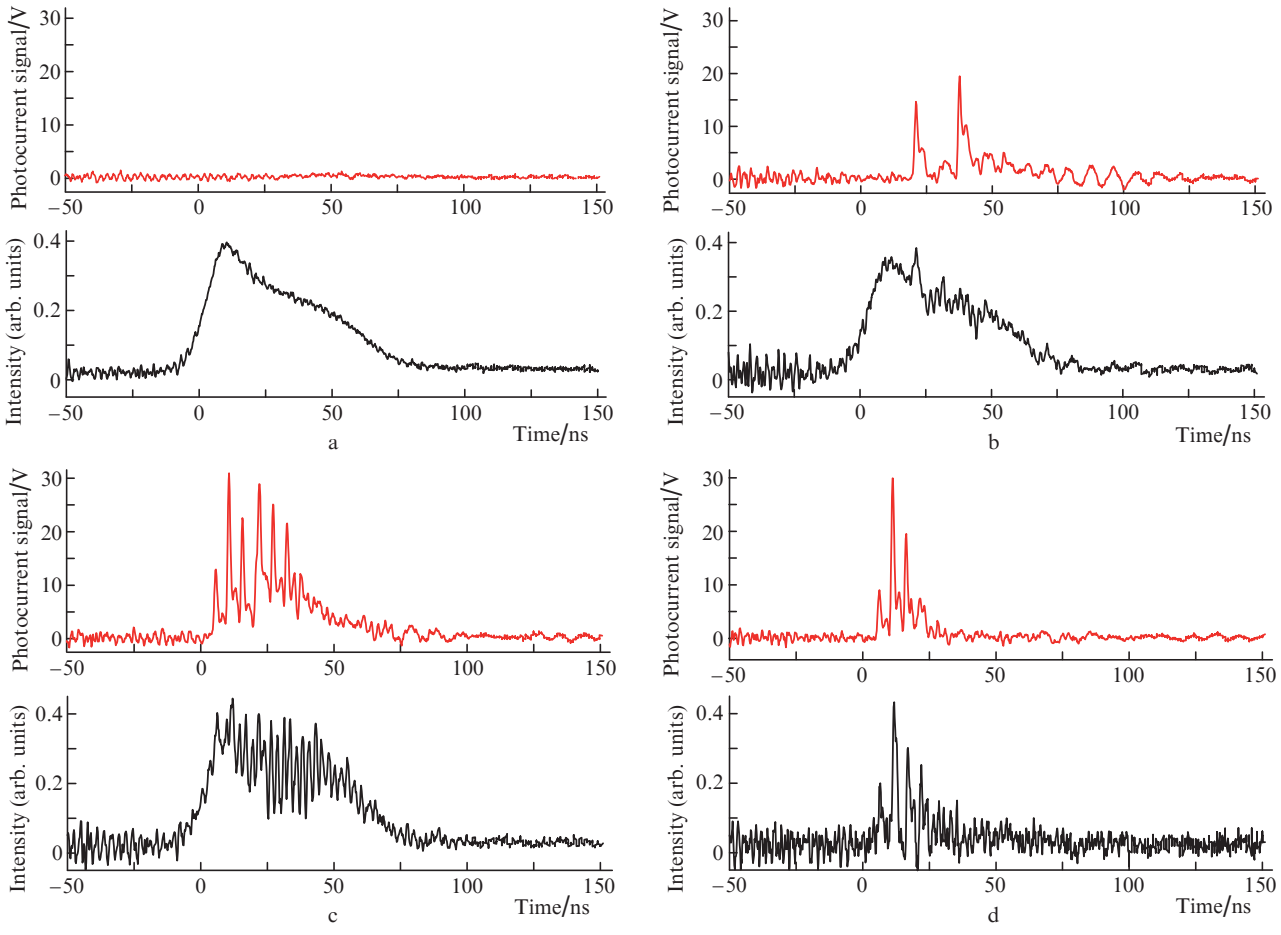

Figure 2. Waveforms of laser pulses and photocurrent without USP injection into the resonator (a), in the injection of a single USP (b) and a USP train (c) into the resonator, as well as in the injection of a USP train into a misaligned resonator (d). The USP amplitudes in the waveforms (b–d) of laser pulses are underrated by a factor of 1000 owing to the insufficient temporal photodetector resolution.

time in the active medium, was injected into the resonator, at the regenerative amplifier output we observed a pulse with a strong amplitude-time modulation. The USPs circulating in the resonator largely suppressed the quasi-continuous lasing, because spacing between the USPs was less than the characteristic lasing development time [37]. Apart from the corresponding increase in peak repetition rate, the photocurrent signals showed an increase in peak amplitudes up to 30 V; there also emerged a pedestal between the peaks, which was 3–5 times lower than the highest amplitude value. The emergence of a constant photocurrent component evidently testifies to accumulation of electrons in the plasma due to the suppression of electron attachment to oxygen molecules by the radiation of quasi-continuous lasing (Fig. 2c). We emphasise that the energy and total duration of the laser pulse remain approximately the same in all cases described above [37]. Lastly, misaligning the output meniscus mirror of the regenerative amplifier transformed it to an ordinary double-pass amplifier, in which the output radiation reproduced the shape of the input USP train. The number of amplified USPs, their total energy, and the total duration of the output radiation pulse decreased in this case. The photocurrent signal consisted of several peaks with amplitudes of up to 30 V, but the pedestal between the peaks turned out to be much lower than in the previous case, because there was no quasi-stationary lasing, which provided electron photodetachment from negative oxygen ions (Fig. 2d). Therefore, our experiments have demonstrated a high efficiency of air ionisation by amplitude-modulated UV radiation pulses. The plasma conductivity and electron density produced by the combined pulses turned out to be at least 100 times higher than for smooth pulses with the same energy and duration.

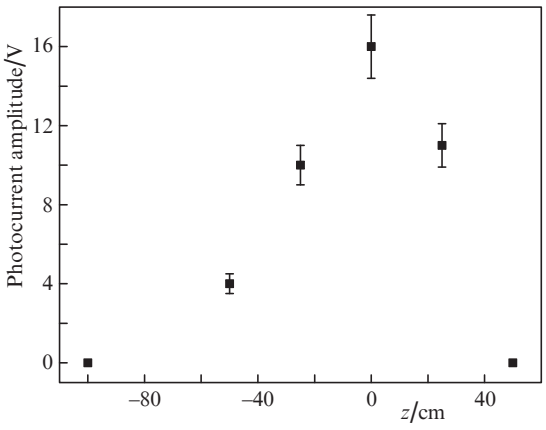

Figure 3. Dependence of the photocurrent amplitude on the position of the geometrical focus of the system. The uncertainties were determined by the statistical spread of measurement data.

For a given focusing of the laser beam, the length of the plasma channel was determined by changing the position of the geometrical focus of the system relative to the interelectrode gap. Figure 3 depicts the dependence of the photocurrent amplitude on the position of the geometrical focus. In this case, the voltage across the gap was equal to 5 kV, the regenerative amplifier was operating in the regime of USP train injection, and coordinate $z = 0$ corresponded to geometrical focus location at the distant grounded electrode (see Fig. 1). One can see that the plasma photocurrent is recorded over a length of ~100 cm, which is consistent with our previous measurements for plasmas produced by single USPs [42].

From photocurrent measurements it is possible to find the conduction of the plasma channel and, knowing its cross section equal to the cross section of the laser beam, the plasma conductivity. The energy density distribution for the laser beam was measured from the UV radiation-induced fluorescence of a thin glass plate, which was imaged onto a Videoskan-285 digital CCD camera. Figure 4 shows the profiles of laser beam intensity recorded in this way. The beam images were obtained for a single USP and a train of USPs amplified in the double-pass scheme when the output meniscus mirror of the resonator was misaligned (see Fig. 2d). Multiple radiation filamentation was observed in all beam cross sections, although it was smoother in the cross section behind the geometrical focus. However, no extended domain of nonlinear beam focusing is observed the geometrical focus, unlike the case of IR radiation. For a USP train, the nonuniformity of the distributions is somewhat stronger than for single USPs because of the interaction between the subsequent USPs and the plasma filaments produced by the preceding pulses.

The average beam diameter increased approximately three-fold at distances of 50 cm from the focus on either side. The focal waist length in which the beam diameter changed only slightly was equal to ~40 cm. For a focal spot diameter of 1 mm, the corresponding area $S = 0.8 \times 10^{-2}$ cm^2, and a peak USP power of 0.2–0.3 TW we obtain a peak radiation intensity of $(2.5–3.8) \times 10^{13}$ W cm^{-2} in the waist domain. To estimate the plasma conductivity, from Fig. 3 we find that the highest photocurrent signal of 15 V ($z = 0$) at the 50-Ω oscilloscope input corresponds to a photocurrent $I_{max} = 0.3$ A in

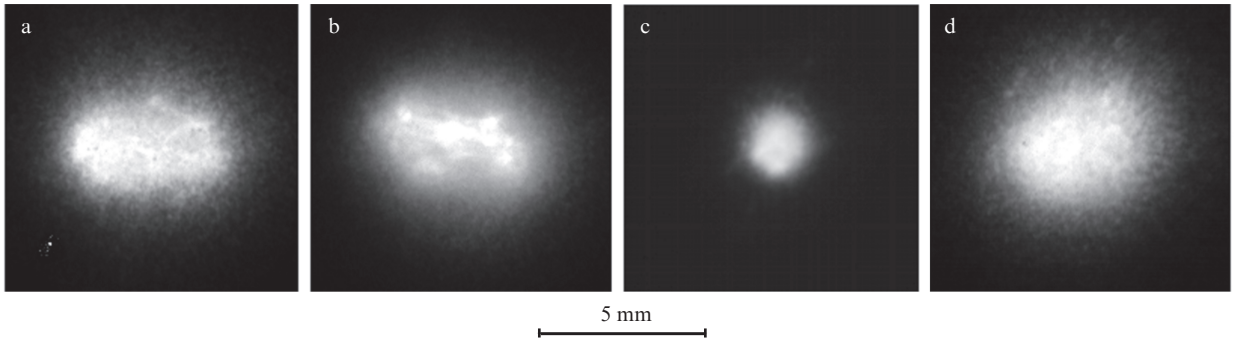

Figure 4. Energy density distribution for a USP of UV laser radiation at a distance of 50 cm ahead of the geometrical focus (a, b), at the focus (c), and 50 cm behind the geometrical focus (d); (a) and (d) are distributions for a single pulse and (b) and (c) for a train of USPs.

the plasma channel; in this case, the channel resistance $R = U/I_{max} = 17$ k Ω^{-1} and the plasma conductivity $\sigma_{e\,max} = L/RS = 0.16\ (\Omega\,cm)^{-1}$. Hence one can find the electron plasma density $n_{e\,max} = \sigma_{e\,max}/e\mu_e \approx 1.6 \times 10^{15}$ cm^{-3} corresponding to the peak photocurrent signal, where the electron mobility μ_e in the atmospheric air is assumed to be equal to 600 cm^2(V s)$^{-1}$ [44, 45]. We note that the local electron density in the filaments may by an order of magnitude higher than the density value found by averaging over the focal spot [12–14]. Furthermore, owing to insufficiently high temporal resolution of the photoelectric circuit (~1 ns), the measured electron density $n_{e\,max}$ is significantly lower than its peak value n_{e0} at the instant of USP passage. Therefore, the electron density induced by the USPs satisfies the condition $n_{e0} \gg n_{e\,max} \geqslant n_e^* = 10^{14} \times 10^{15}$ cm^{-3}, whose fulfilment signifies that the photoionisation plasma is dominated by electron-ion recombination with the characteristic electron loss time of the order of several nanoseconds (see Section 1). A similar estimate for the constant photocurrent component suggests that the electron density $n_e = (3–5) \times 10^{14}$ cm$^{-3} \approx n_e^*$; for this density, electron attachment to oxygen becomes the main relaxation process. Electron photodetachment from O_2^- molecular ions by quasi-stationary lasing radiation suppresses attachment and maintains the electron density at a quasi-stationary level throughout the action of a amplitude-modulated laser pulse (~100 ns).

3. Switching and control of high-voltage electric discharges in the air by amplitude-modulated UV radiation pulses

Described in this Section are experiments intended to verify the conception of efficient control of high-voltage electric discharges in atmospheric air by amplitude-modulated UV laser radiation pulses. This conception relies on the production of electrons in photoionisation plasma due to multiphoton air ionisation by a train of USPs amplified to subterawatt power and the maintaining of their density by suppressing electron attachment to oxygen molecules with the use of a 100-ns long quasi-continuous lasing pulse.

3.1. Discharges at constant voltage across a discharge gap

For experiments in high-voltage discharge triggering at a constant voltage across the discharge gap we used a circuit with two IMN-100-0.1 high-voltage capacitors with a capacity of 0.1 μF, which were charged to a voltage, controllable up to U = 70 kV, from two rectifiers of opposite polarity (Fig. 5a). In this case, a doubled voltage up to $\Delta U = 2U$ = 140 kV was applied to the discharge gap formed by two spherical electrodes of radius 1.5 cm. UV laser radiation pulses with an energy of ~6 J, a duration of 100 ns and different temporal structure (smooth and amplitude-modulated) were focused by a spherical mirror with a focal distance F = 8 m. A similar focusing was employed in the photoelectric measurements of electron density in the plasma channel (see Section 2). The laser beam passed tangentially to the near (relative to the direction of beam propagation) electrode, and its geometrical focus was located in the discharge gap closer to the distant electrode. The discharge shape was recorded with a Videoskan-285 CCD camera with an acquisition interval of 100 ms. The current was measured with a Rogowski coil; its signal together with the signal from a Thorlabs DET 210 photodiode was recorded with a digital oscilloscope. The photodiode recorded both the laser pulse and the glow of discharge plasma. By comparing their waveforms we determined the delay of discharge ignition relative to the laser pulse.

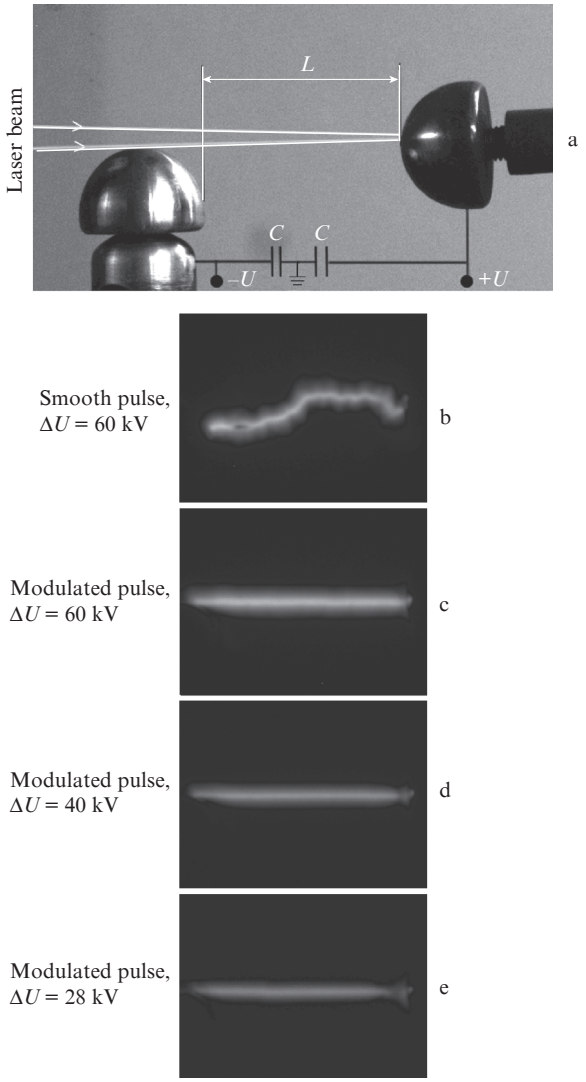

Figure 5. Schematic of experiments in high-voltage discharge triggering at a constant voltage (a), as well as discharge images for a smooth laser pulse (b) and amplitude-modulated pulses (c–e).

For a fixed interelectrode distance L = 8.0 cm, the applied voltage was varied in the range between the self-breakdown voltage (i.e. without application of a laser pulse) and the threshold of laser triggering both for smooth and amplitude-modulated laser pulses with equal energies. The self-breakdown was inherently stochastic and was observed in the voltage range ΔU_{br} = 80–100 kV, which corresponded to an average electric intensity $E_{br} = \Delta U_{br}/L$ =10–12.5 kV cm^{-1} in the gap. This figure is somewhat lower than that obtained in our previous experiments with a short discharge gap (L = 1.5 cm), where the breakdown voltage was ΔU_{br} = 50 kV [38, 42]. The difference is supposedly due to a higher field uniformity and a lower humidity of laboratory air in the experiments of Refs [38, 42], which were carried out in winter. For a gap with L = 8 cm, the threshold of laser triggering by modulated pulses (i.e. the minimal voltage whereby the breakdown still developed with a probability close to 100%) was ΔU_{trig} = 28 kV, which was three times lower than the self-breakdown thresh-

old ΔU_{br}. It is significant that the discharge was guided along the laser beam (Figs 5c and 5d). The delay of discharge ignition relative to the laser pulse was less than 0.3 μs for higher voltages and about 10 μs near the triggering threshold ΔU_{trig}. For a smooth laser pulse with the same energy, the breakdown of the same gap occurred for a significantly higher voltage ($\Delta U_{trig} \approx 60$ kV), developed along a random trajectory (Fig. 5b) and for a very long delay relative to the laser pulse, which ranged up to 400–500 μs.

3.2. Extended discharges under a pulsed voltage across the discharge gap

Figure 6 shows the experimental setup for the laser triggering of extended (~1 m) high-voltage discharges under a pulsed voltage applied to the discharge gap between a small charged sphere and a plane. The laser beam was focused in the geometry described above and, using a plane deflecting mirror, was directed to the discharge gap through a 4-cm diameter hole in a plane grounded disc 70 cm in diameter. A seven-stage Marx pulsed voltage generator (PVG) made up of IMN-100-0.1 capacitors generated voltage pulses with an amplitude of up to 490 kV, which were applied to the spherical 3-cm diameter electrode with an adjustable time delay τ_{del} relative to the laser pulse (Fig. 7). The discharge current was measured with a Rogowski coil and the PVG voltage was measured with another Rogowski coil, which encircled a low-inductance load with a resistance of 2 kΩ connected in parallel with the discharge gap. The instant of gap breakdown was recorded on waveforms as an abrupt rise in the current signal and a simultaneous voltage drop (Fig. 7). A low current preceding the breakdown (or at all in the absence of breakdown) was due to the discharge of the PVG through its charging resistors (they are not shown in Fig. 6). The discharge shape was recorded with the CCD camera with an acquisition interval of 100 ms (Fig. 8).

The breakdown of a ~70-cm long discharge gap for a PVG voltage of 420 kV was observed only for amplitude-modulated pulses, whose energy measured 6.3 J in these experiments. We measured the discharge development time

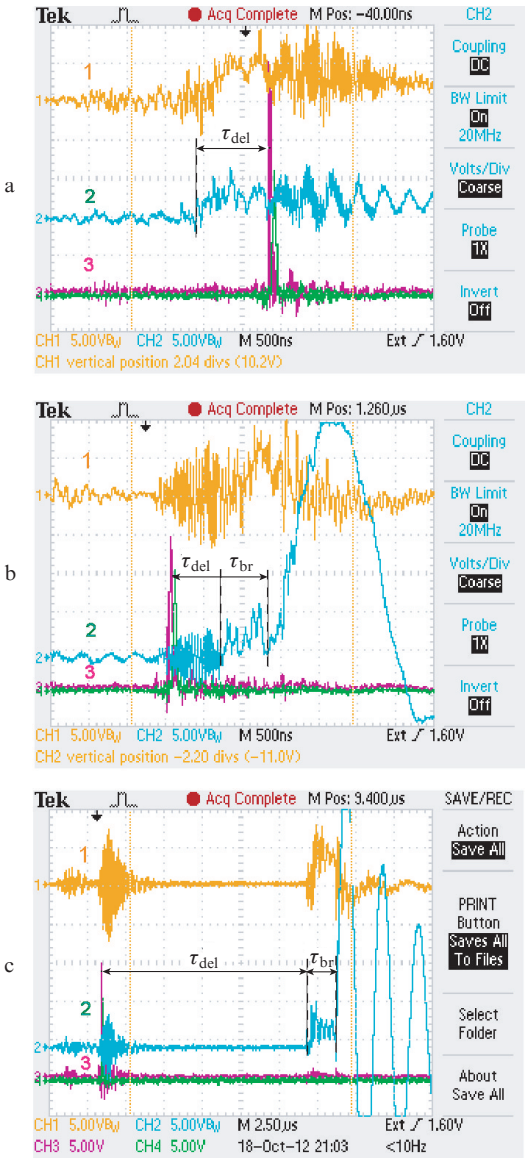

Figure 7. Waveforms of discharge voltage (1) and current (2) as well as of laser pulses (3) for different delays between the laser pulse and the PVG pulse for sweep speeds of 0.5 (a, b) and 2.5 μs per division (c). In the case of Fig. 7a, the PVG pulse arrives ahead of the laser pulse and no breakdown occurs.

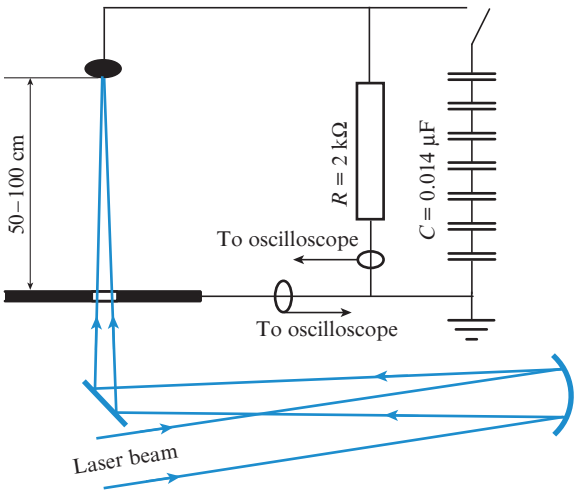

Figure 6. Layout of the experiments in the triggering of a high-voltage discharge for a pulsed voltage across the gap between a sphere and a plane.

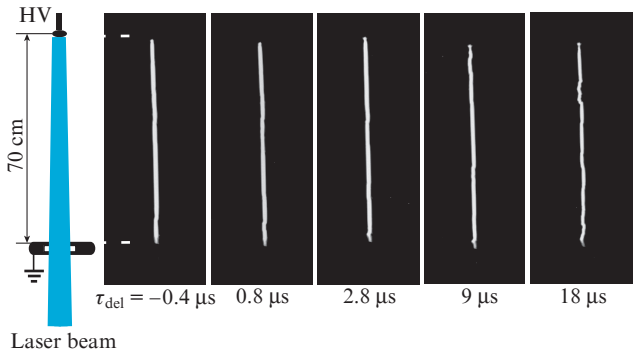

Figure 8. Images of discharges initiated by an amplitude-modulated laser pulse in a 70-cm long interelectrode gap for different time delays between the laser pulse and the PVG pulse.

τ_{br}, which was counted from the instant of high-voltage pulse application until the instant of breakdown, as a function of the time delay τ_{del} of the voltage pulse relative to the laser pulse (Fig. 9). The minimal breakdown development time $\tau_{br} \approx 0.6$ μs corresponded to a time delay $\tau_{del} \approx 0.8$ μs. With increase in delay to $\tau_{del} \approx 18$ μs the discharge development time increased to τ_{br}=3.7 μs. No breakdown occurred for higher time delays owing to a PVG pulse voltage drop resulting from leakage through the charging resistors. Also, no breakdown occurred when the high-voltage pulse was applied more than 1 μs earlier than the laser pulse ($\tau_{del} = -1$ μs in Fig. 9). The reason may lie with a redistribution of the electric field in the gap prior to the arrival of the laser pulse. In all remaining cases the discharge initiated by the amplitude-modulated laser pulse was guided along the laser beam. The small parallel discharge trajectory displacements observed in Fig. 8 evidently testify to a stepwise discharge leader propagation.

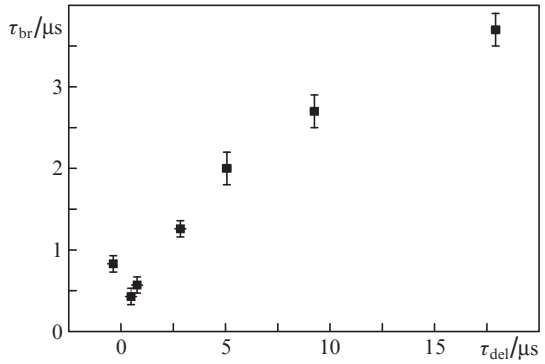

Figure 9. Dependence of the discharge development time on the time delay between the application of the voltage pulse and the laser pulse.

4. Hypothesised mechanism of laser discharge triggering

The long electric breakdown development times – tens and even hundreds of microseconds, which were observed in experiments with a constant voltage across the discharge gap as well as in experiments with high-voltage pulses delayed relative to the laser pulse, are many orders of magnitude longer than the free-electron lifetime in the laser plasma. Proceeding from the derived data, we can propose the following mechanism for high-voltage discharge triggering by amplitude-modulated UV laser radiation. Free electrons in the air plasma are produced by way of direct or stepwise multiphoton ionisation of oxygen molecules by a USP train and for a high initial density ($n_{e0} \gg 10^{15}$ cm^{-3}) rapidly, within nanoseconds, recombine with the O_2^+ positive ions. As the electron density lowers to $n_e = (3-5)\times 10^{14}$ cm^{-3}, electron attachment to oxygen molecules with the production of O_2^- molecular ions begins to dominate. Quasi-continuous UV radiation suppresses this process due to the resonance photodetachment of electrons from the O_2^- molecular ions. The USPs in combination with the 100-ns long quasi-continuous lasing pulse, which form an amplitude-modulated pulse, produce electrons 100 times more efficiently than a smooth radiation pulse of the same duration and energy. Upon termination of the laser pulse, the electrons attach to O_2 molecules within several tens of nanoseconds (this time depends on the magnitude of the applied electric field). The O_2^- molecular ions, which possess a very low binding energy (~0.5 eV), are easily ionised in the applied electric field. The electric air breakdown develops as a result of avalanche ionisation with participation of this easily ionisable component and depends on the electric intensity and the O_2^- ion density, i.e. on the number of photoelectrons accumulated during the course of the laser pulse. Therefore, the breakdown development time is limited not by the free-electron lifetime, but by the recombination time between the O_2^- negative ions and the O_2^+ and O_4^+ positive ions, which is equal to ~1 ms [45]. The stepwise character of discharge leader propagation is supposedly due to electric charge redistribution along the plasma channel covered by the leader and the corresponding electric field sharpening at the ends of this segment [6].

5. Conclusions

The experiments carried out in the present work have shown that amplitude-modulated UV radiation pulses, being the superposition of a USP train amplified in a regenerative KrF amplifier to a peak power of 0.2–0.3 TW and a 100-ns long quasi-steady lasing pulse, offer significant advantages over smooth pulses or a USP train for the production of extended plasma channels in the atmospheric air, and for the triggering and control of high-voltage electric discharges. The USPs efficiently ionise oxygen molecules by way of direct or stepwise multiphoton ionisation, while the quasi-steady lasing pulse maintains the electric density by suppressing electron attachment to oxygen. In experiments on the laser triggering of high-voltage electric discharges we have demonstrated that the use of amplitude-modulated pulses results in a significant lowering of the breakdown threshold and a higher-efficiency control of discharge trajectory in comparison with the use of smooth pulses. We have shown that controlled discharge may develop with a delay of tens of microseconds relative to the laser pulse; this time is many orders of magnitude longer than the free-electron lifetime in the laser plasma. A mechanism has been proposed for this breakdown, which involves speeding-up of the avalanche ionisation of the air by negative molecular oxygen ions with a low electron binding energy (~0.5 eV) and a long lifetime (~1 ms), which are produced upon cessation of the laser pulse.

Acknowledgements. This work was supported by the programmes 'Extreme Light Fields and Their Applications' and 'Fundamental Problems of Pulsed High-Current Electronics of the Presidium of the Russian Academy of Sciences, by the Russian Foundation for Basic Research (Grant Nos 11-02-01414, 11-02-01524, 11-02-12061-ofi-m, and 12-02-31431-mol_a), as well as by the EOARD (Grant No. 097007) in the framework of the ISTC Partner Project No. 4073 R.

References

1. Danilychev V.A., Zvorykin V.D. *Trudy Fiz. Inst. Akad. Nauk SSSR*, **142**, 117 (1983).
2. Zvorykin V.D., Nikolaev F.A., Kholin I.V., et al. *Fiz. Plazmy*, **5**, 1140 (1979).
3. Apollonov V.V., Vasilyak L.M., Kazantsev S.Yu., et al. *Kvantovaya Elektron.*, **32** (2), 115 (2002) [*Quantum Electron.*, **32** (2), 115 (2002)].

4. Grachev G.N., Ponomarenko A.G., Smirnov A.L., et al. *Kvantovaya Elektron.*, **35** (11), 973 (2005) [*Quantum Electron.*, **35** (11), 973 (2005)].
5. Apollonov V.V., Pletnev N.V. *Kvantovaya Elektron.*, **42** (2), 130 (2012) [*Quantum Electron.*, **42** (2), 130 (2012)].
6. Bazelyan E.M., Raizer Yu.P. *Fizika molnii i molniezashchita* (The Physics of Lightning and Lightning Protection) (Moscow: Fizmatlit, 2001).
7. Wille H., Rodriguez M., Kasparian J., et al. *Eur. Phys. J. Appl. Phys.*, **20**, 183 (2002).
8. http://www.teramobile.org/publis.html.
9. Zhao X.M., Wang Y.C., Diels J.-C., Elizondo J. *IEEE J. Quantum Electron.*, **31**, 599 (1995).
10. Zvorykin V.D., Ionin A.A., Levchenko A.O., et al. *J. Phys. Conf. Ser.*, **244**, 032014 (2010).
11. Zvorykin V.D., Levchenko A.O., Ustinovskii N.N. *Kvantovaya Elektron.*, **40** (5), 381 (2010) [*Quantum. Electron.*, **40** (5), 381 (2010)].
12. Berge L., Skupin S., Nuter R., et al. *Rep. Progr. Phys.*, **70**, 1633 (2007).
13. Couairon A., Mysyrowicz A. *Phys. Rep.*, **441**, 47 (2007).
14. Kandidov V.P., Shlenov S.A., in *Glubokoe kanalirovanie i filamentatsiya moshchnogo lazernogo izlucheniya v veshchestve* (Deep Channeling and Filamentation of High-Power Laser Radiation in Substance) (Moscow: Interkontakt Nauka, 2009) pp 185–266.
15. La Fontaine B., Vidal F., Comtois D., et al. *IEEE Trans. Plasma Sci.*, **27**, 688 (1999).
16. Vidal F., Comtois D., Chien C.Y., et al. *IEEE Trans. Plasma Sci.*, **28**, 418 (2000).
17. Desparois A., La Fontaine B., Bondiou-Clergerie A., et al. *IEEE Trans. Plasma Sci.*, **28**, 1755 (2000).
18. Comtois D., Chien C.Y., Desparois A., et al. *Appl. Phys. Lett.*, **76**, 819 (2000).
19. Pepin H., Comtois D., Vidal F., et al. *Phys. Plasmas*, **8**, 2532 (2001).
20. Rodriguez M., Saurbrey R., Wille H., et al. *Opt. Lett.*, **27**, 772 (2002).
21. Comtois D., Pepin H., Vidal F., et al. *IEEE Trans. Plasma Sci.*, **31**, 377 (2003).
22. Gordon D.F., Ting A., Hubbard R.F., et al. *Phys. Plasmas*, **10**, 4530 (2003).
23. Ackerman R., Mechain G., Mejean G., et al. *Appl. Phys. B*, **82**, 561 (2006).
24. Ackerman R., Stelmaszczyk K., Rohwetter P., et al. *Appl. Phys. Lett.*, **85**, 5781 (2006).
25. Aleksandrov N.L., Bazelyan E.M., Bogatov N.A., et al. *Fiz. Plazmy*, **34**, 1142 (2008).
26. Fujii T., Miki M., Goto N., et al. *Phys. Plasmas*, **15**, 013107 (2008).
27. Sugiyama K., Fujii T., Yamaguchi M., et al. *Opt. Lett.*, **34**, 2964 (2009).
28. Forestier B., Houard A., Revel I., et al. *AIP Advances*, **2**, 012151 (2012).
29. Yang H., Zhang J., Li Y.J., et al. *Phys. Rev. E*, **66**, 016406 (2002).
30. Zhu J., Ji Z., Deng Y., et al. *Opt. Express*, **14**, 4915 (2006).
31. Mejean G., Ackerman R., Kasparian J., et al. *Appl. Phys. Lett.*, **88**, 021101 (2006).
32. Zvorykin V.D., Levchenko A.O., Shutov A.V., et al. *Phys. Plasmas*, **19**, 033509 (2012).
33. Hao Z.Q., Zhang J., Li Y.T., et al. *Appl. Phys. B*, **80**, 627 (2005).
34. Zhou B., Akturk S., Prade B., et al. *Opt. Express*, **17**, 11450 (2009).
35. Polynkin P., Moloney J.V. *Appl. Phys. Lett.*, **99**, 151103 (2011).
36. Shneider M.N., Zheltikov A.M., Miles R.B. *Phys. Plasmas*, **18**, 063509 (2011).
37. Zvorykin V.D., Ionin A.A., Levchenko A.O., et al. *Kvantovaya Elektron.*, **43** (4), 332 (2013) [*Quantum. Electron.*, **43** (4), 332 (2013)].
38. Zvorykin V.D., Ionin A.A., Levchenko A.O., et al. *Nucl. Instrum. Methods Phys. Res., Sect. B* (in print).
39. Couairon A., Berge L. *Phys. Rev. Lett.*, **88**, 135003 (2002).
40. Hodges R.V., Lee L.C., Moseley J.T. *J. Chem. Phys.*, **75**, 2998 (1980).
41. Ling P., Lucchese R.R. *J. Chem Phys.*, **114**, 9350 (2001).
42. Ionin A.A., Kudryashov S.I., Levchenko A.O., et al. *Appl. Phys. Lett.*, **100**, 104105 (2012).
43. Zvorykin V.D., Levchenko A.O., Ustinovskii N.N. *Kvantovaya Elektron.*, **41** (3), 227 (2011) [*Quantum Electron.*, **41** (3), 227 (2011)].
44. Huxley L.G.H., Crompton R.W. *The Diffusion and Drift of Electrons in Gases* (New York: Wiley, 1974; Moscow: Mir, 1977).
45. Raizer Yu.P. *Gas Discharge Physics* (Berlin: Springer, 1991; Moscow: Nauka, 1987).